Electroproduction of the Roper resonance on the proton: The role of the three-quark core and the molecular $N\sigma$ component

Igor T. Obukhovsky,[1] Amand Faessler,[2] Dimitry K. Fedorov,[1] Thomas Gutsche,[2] and Valery E. Lyubovitskij[2,*]

[1]*Institute of Nuclear Physics, Moscow State University,119991 Moscow, Russia*
[2]*Institut für Theoretische Physik, Universität Tübingen, Kepler Center for Astro and Particle Physics,*
Auf der Morgenstelle 14, D-72076 Tübingen, Germany

The Roper resonance is considered as a mixed state of a three-quark core configuration and a hadron-molecular component $N + \sigma$. Based on this ansatz we study electroproduction of the Roper resonance. The strong and electromagnetic couplings induced by the quark core are calculated in the $^3P_0$ model. The contribution of the vector-meson cloud to the electromagnetic transition is given in the framework of the vector-meson dominance model. Results are compared with the recent JLab electroproduction data.

I. INTRODUCTION

The structure issue of the lowest lying nucleon resonance $N(1440)$ with $J^P = \frac{1}{2}^+$ (the Roper resonance P_{11} or simply R) has been a long standing problem of hadron physics. One of the indication that the inner structure of the Roper is possibly more complicated than the structure of the other lightest baryons was obtained some time ago in the framework of the constituent quark model (CQM). It was found (see, e.g., [1]) that the observed mass of the Roper resonance is much too low and the decay width is too large when compared to the predicted values of the CQM.

The simplest description of the Roper consists of the three-quark $(3q)$ configuration $sp^2[3]_X$, i.e., the first $(2S)$ radial excitation of the nucleon ground state $s^3[3]_X$, but it fails to explain either the large decay width $\Gamma_R \simeq 300$ MeV or the branching ratios for the πN (55%–75%) and σN (5%–20%) decay channels [2,3]. Evaluation of these values in the framework of the CQM is often based on the elementary-emission model (EEM) with single-particle quark-meson (or quark-gamma) couplings $qq\pi$, $qq\sigma$, $qq\gamma$, etc. The calculation of decay widths (or of the electroproduction cross section at small virtuality of the photon with $Q^2 \simeq 0$) results in anomalous small values. These underestimates can especially be traced to the strict requirement of orthogonality for the ground $(0S)$ and excited state $(2S)$ radial wave functions of the N and R states belonging to the quark configurations with the same spin-isospin $(S = 1/2$, $T = 1/2)$ and symmetry $([3]_{ST}[3]_X)$ quantum numbers. To overcome this discrepancy it is suggested that either the Roper is not an ordinary $3q$ state or the "true" transition operators have a more complicated form than the single-particle operators used in calculations.

Quark models with Goldstone boson interactions [4] can explain why the mass of the Roper resonance is shifted to the observed value including the correct level ordering. But

these models still fail to get the strong decay widths and electromagnetic couplings under control.

On the experimental side there has been noticeable progress in the experimental study of the Roper resonance in the last decade. The Roper resonance has been studied in π [5] and $\pi\pi$ [6] electroproduction processes on the proton with the polarized electron beam at the JLab (CLAS Collaboration) followed by a combined analysis of pion- and photo-induced reactions made by CB-ELSA and the A2-TAPS Collaborations [3]. These recent data present new possibilities for the study of the lightest baryon resonances.

Several models for the description of the Roper resonance electroexcitation were proposed during the last three decades [7–16] (see the review [17] for a detailed discussion). Now model predictions can be compared with the new high-quality photo- and electroproduction data [3,5,6], and updated versions [18–20] of the most realistic models give a good description of the data at intermediate values of $1.5 \lesssim Q^2 \lesssim 4$ GeV^2. However, in the "soft" region, i.e., at low values of Q^2 ($0 \leq Q^2 \lesssim 1$–1.5 GeV^2), the data differ qualitatively from the theoretical predictions: the experimental helicity amplitude $A_{1/2}$ changes sign at $Q^2 \approx 0.5$ GeV^2 and it is large and negative at the photon point $Q^2 = 0$. Theoretical predictions for $A_{1/2}$ are large and positive at $Q^2 \approx 0.5$ GeV^2 and quickly go to a small negative (or zero) value at the photon point.

For pion electroproduction in the resonance region $W \simeq m_R$ the behavior of the transverse helicity amplitude $A_{1/2}$ near the photon point $Q^2 \gtrsim 0$ is most sensitive to the soft component of the resonance state, i.e., to the possible contribution of the meson cloud. Electroproduction amplitudes in this kinematical region are successfully analyzed in terms of the dynamical coupled channel model [21,22], which is used at the Excited Baryon Analysis Center at JLab (see, e.g., [23]). The detailed description of the low-Q^2 CLAS $p\pi^+\pi^-$ data [24] was obtained in Ref. [6] on the basis of JLab-Moscow model [25,26] with taking into account the $\pi\Delta$ channel along with additional

_____
*On leave of absence from Department of Physics, Tomsk State University, 634050 Tomsk, Russia.

contact terms and the direct 2π production. The contribution of the meson (pion) cloud to the Roper resonance mass was recently calculated in Refs. [27,28].

As a result, there are essentially two comprehensive theoretical approaches to the Roper electroproduction on the market. One of them (the coupled channel model of the meson cloud [6,21–23]) is only successful in the soft region $0 \leq Q^2 \lesssim 1$ GeV^2 and the other one [the light front (LF) three-quark model [12,18] or the covariant quark spectator model [19]] is compatible with data in the hard region $1.5 \lesssim Q^2 \lesssim 4$ GeV^2.

Universal, but more phenomenological approaches which pretend to cover both regions of Q^2 were also suggested (see, e.g., Refs. [15,20]). In Ref. [15] a $3q + \bar{q}q$ approach was suggested using the $^3P_0$ model [7] and vector-meson dominance (VMD) in combination with the EEM. In Ref. [20] a generalization of the cloudy bag model [29] was used for the case of the open inelastic channels $\pi\Delta$ and σN in combination with a phenomenological strong background interaction.

In such combined approaches two types of electromagnetic transition operators are used, the operator designed for the soft Q^2 region and one for hard values of Q^2. However, in the transition amplitude they are summed for any value of Q^2. For example, in the generalized $^3P_0 +$ EEM approach [15] the transition operator includes the sum of two vertices, schematically sketched in Figs. 1(a) and 1(b).

In the present paper we follow a more physical concept (see, e.g., Ref. [30] where the constituent quark and parton approaches to the γqq vertex are discussed in the context of the nucleon electromagnetic form factors). We can consider that the diagram in Fig. 1(a) represents the unknown large-distance physics described by a phenomenological model (the $^3P_0$ model in our case), which is adjusted to low-energy data (i.e. meson-nucleon coupling constants πNN, ρNN, magnetic moments, and decay widths). In the hard Q^2 region these contributions become less important and an adequate description of the electromagnetic transition will be given by the diagram in Fig. 1(b). In this case the unknown short-range physics is encoded by the adjusted parameters of a parton model. In the region of moderate values of Q^2 ($1.5 \lesssim Q^2 \lesssim 4$ GeV^2) we can consider the constituent quarks as partons and corresponding unknown short-range physics can be included in a few constituent quark parameters (such as quark form factors
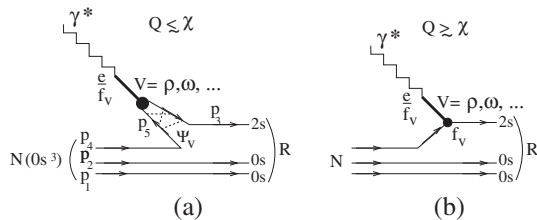
given by the intermediate vector mesons in the VMD model and scale parameters of quark configurations in the baryons). In this case it is not necessary to sum the contributions of the two diagrams in Fig. 1. Instead it would be desirable to use some mechanism for a smooth transition from one regime to the other.

In our opinion such a mechanism can be described in general by a smooth transition from a typical hadron radius $b_V \approx 0.5$ fm of the vector meson in the CQM to a pointlike vector meson $b_V = 0$ corresponding to the quark-parton picture sketched in Fig. 1(b). Here we use the approximation $b_V(Q^2) = b_V(0)e^{-Q^2/\chi^2}$, where $\chi \simeq 1$–2 GeV corresponds to the lowest characteristic value of Q^2 where the parton model phenomenology in deep inelastic ep scattering sets in.

Another important issue related to the Roper resonance is a possible combined structure of this state which implies a virtual hadron-hadron component (e.g. σN or/and $\pi\Delta$) [31] in addition to the radially excited three-quark structure. Here we consider an admixture of the hadronic molecular state $N + \sigma$ in an effective description of such a component. We also consider to what degree such a combined structure for the Roper is compatible with the new high-quality data of JLab.

II. COMPOSITE STRUCTURE OF THE ROPER RESONANCE

We consider the Roper resonance (R) as a superposition of the radially excited three-quark configuration $3q^*$ and the hadron molecule component $N + \sigma$ as

$$|R\rangle = \cos\theta|3q^*\rangle + \sin\theta|N + \sigma\rangle, \tag{1}$$

where θ is the mixing angle between the $3q^*$ and the hadronic component: $\cos^2\theta$ and $\sin^2\theta$ represent the probabilities to find a $3q^*$ and hadronic configuration, respectively. The parameter θ is adjusted to optimize the description of data on the Roper resonance electroproduction. The limiting case of $\cos\theta = 1$ corresponds to the pure $3q^*$ interpretation of R, while the value $\cos\theta = 0$ corresponds to the situation, where R is a pure loose bound state of $N + \sigma$ (analogous to the deuteron-bound state of proton and neutron). Note, in a first step we simplify the model by reducing it to two independent (decoupled) systems, $R_1 = 3q^*$ and $R_2 = N + \sigma$, and do not consider the full coupled channel problem. Moreover, we consider the dynamics of the R_1 component in the framework of the nonrelativistic $^3P_0$ model (see, e.g., Refs. [7,32]), while the dynamics of the R_2 component is considered in the framework of the hadronic molecular approach [33] which is manifestly Lorentz invariant. In the future we intend to improve the description of the R_1 component by applying a relativistic quark model.

First, we briefly outline the basic notions of the $^3P_0$ model. The effective interaction term of the $^3P_0$ model [32,34] is set up as

FIG. 1. Diagrams of (a) soft (nonlocal) and (b) hard (local) coupling of vector mesons to the nucleon quark core.

$$H_q^{\text{eff}} = g_q \int d^3x \, \bar{\psi}_q \psi_q, \qquad g_q = 2m_q \gamma, \qquad (2)$$

where γ is dimensionless constant. It can be considered as a static variant of the coupling $\gamma' \bar{q}(x) q(x) S(x)$ where the external field $S(x)$ represents some scalar combination of gluon fields in the hadron. At low energy, where the dynamics is ruled by nonperturbative QCD, we pass to an effective description in terms of constituent quarks $\psi_q(x)$ and substitute a constant for the field $S(x)$.

Apart from some drawbacks [see, e.g., Eqs. (B2) and (B3) in Appendix B], the $^3P_0$ model [32,35,36] is a good phenomenological method for the evaluation of hadron transitions [37–40] on the basis of the quark model starting from Eq. (2) with a single strength parameter γ. The interaction term (2) gives rise to Feynman amplitudes for the $\bar{q}q$ pair creation (annihilation)

$$(2\pi)^3 \delta^{(3)}(\mathbf{p}_4 + \mathbf{p}_5) i \mathcal{M}_{fi}^{\text{eff}}$$
$$= \langle q, \mathbf{p}_4, \mu_4 | \langle \bar{q}, \mathbf{p}_5, \mu_5 | i \int d^3x \, \mathcal{L}_q^{\text{eff}}(x) | 0 \rangle, \qquad (3)$$

which are used here for the calculation of meson-baryon couplings. The quark is labeled by its 3-momentum $\mathbf{p}_4$ and spin projection μ_4 (for simplicity the isospin projection t_4 and the color are omitted), similarly for the antiquark. For the numbering of the quarks see Fig. 1 (or Fig. 8 in Appendix B).

The corresponding nonrelativistic interaction term V_q^{eff} is defined as

$$T_{fi}^{\text{eff}} = {}_{nr}\langle q, \mathbf{p}_4, \mu_4 |_{nr}\langle \bar{q}, \mathbf{p}_5, \mu_5 | V_q^{\text{eff}} | 0 \rangle \doteq \frac{1}{2m_q} \mathcal{M}_{fi}^{\text{eff}}, \quad (4)$$

where a noncovariant normalization

$${}_{nr}\langle \mathbf{p}, \mu | \mathbf{p}', \mu' \rangle_{nr} = (2\pi)^3 \delta^{(3)}(\mathbf{p} - \mathbf{p}') \delta_{\mu,\mu'} \qquad (5)$$

is implied instead of the covariant one of Eq. (3).

Substitution of the nonrelativistic reduction of the effective interaction (2) into Eqs. (3) and (4) leads to the expression

$$V_q^{\text{eff}} \doteq \frac{g_q}{2m_q} (-1)^{1-\mu_5-t_5} \left\langle \frac{1}{2} - \mu_5 \left| \boldsymbol{\sigma} \cdot (\mathbf{p}_4 - \mathbf{p}_5) \right| \frac{1}{2} \mu_4 \right\rangle$$
$$\times \left\langle \frac{1}{2} - t_5 \left| \frac{1}{2} t_4 \right\rangle (2\pi)^3 \delta^{(3)}(\mathbf{p}_4 + \mathbf{p}_5), \qquad (6)$$

which is the nonrelativistic analogue of the $\bar{q}q$ pair creation (annihilation) operator.

The description of the hadronic $N + \sigma$ component of the Roper resonance is based on the compositeness condition [41,42]. This condition implies that the renormalization constant of the hadron wave function is set equal to zero or that the hadron exists as a bound state of its constituents only. In the case of mixed states (as in the present situation where the Roper is a superposition of the $3q^*$ and $N + \sigma$ components) the amplitude for the $N + \sigma$ component is
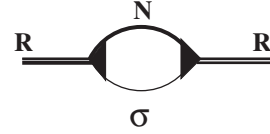

FIG. 2. The $N\sigma$ loop diagram contributing to the Roper mass operator.

defined by the parameter $\sin\theta$. The compositeness condition was originally applied to the study of the deuteron as a bound state of proton and neutron [41]. Then it was extensively used in low-energy hadron phenomenology as the master equation for the treatment of mesons and baryons as bound states of light and heavy constituent quarks (see, e.g., Refs. [42,43]). By constructing a phenomenological Lagrangian including the couplings of the bound state to its constituents and of the constituents to other particles in the possible decay channels we calculated hadronic-loop diagrams describing different decays of the molecular states (see details in [33]).

In the present case the $R_2 \to N + \sigma$ coupling is fixed from the compositeness condition

$$Z_R = 1 - \Sigma'_{N\sigma}(p)|_{\not{p}=m_R} = 0, \qquad (7)$$

where $\Sigma_{N\sigma}(p)$ is the mass operator of the $N\sigma$ bound state (Fig. 2), calculated with the use of the phenomenological Lagrangian

$$\mathcal{L}_R^{\text{str}}(x) = g_{R\sigma N} \bar{R}(x) \int dy \Phi_R(y^2) N(x + w_{\sigma N} y) \sigma(x - w_{N\sigma} y)$$
$$+ \text{H.c.}, \qquad (8)$$

where $w_{ij} = m_i / (m_i + m_j)$. Here $\Phi_R(y^2)$ is the correlation function describing the distribution of $N\sigma$ inside R, which depends on the Jacobi coordinate y. Its Fourier transform used in the calculations has the form of a "modified" Gaussian, i.e., the Gaussian multiplied by a polynomial. In Euclidean space it may be written as

$$\tilde{\Phi}_R(-k_E^2) = \left(1 - \lambda \frac{k_E^2}{\Lambda_M^2}\right) \exp\left(-\frac{k_E^2}{\Lambda_M^2}\right), \qquad (9)$$

where k_E is the Euclidean momentum. This presents a kind of generalization of the nonrelativistic quark model wave function to the 4-dimensional case. But the relativistic parameters λ and Λ_M should differ from the corresponding nonrelativistic ones. Here Λ_M is the molecular size parameter and λ is a free parameter which should be fixed by the orthogonality condition, i.e., $\langle N | R \rangle = 0$.

III. ROPER ELECTROPRODUCTION

The diagrams which contribute to the Roper resonance electroproduction are shown in Fig. 1 (contribution of the $3q^*$ component) and Fig. 3 (contribution of the hadronic $N\sigma$ component). In the following we discuss the separate
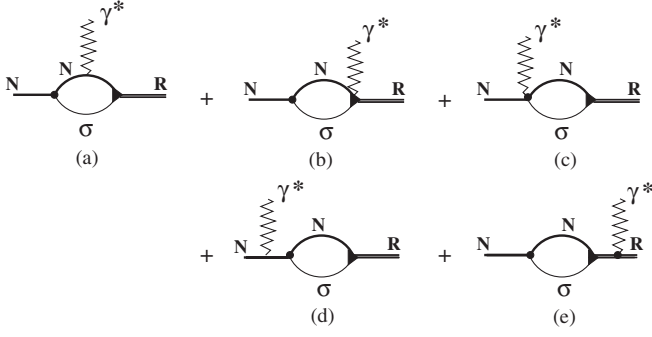
FIG. 3. $N\sigma$ hadronic-loop diagrams contributing to the Roper electroproduction: the triangle diagram (a), the bubble diagrams (b) and (c), the pole diagrams (d) and (e).

contributions of the structure components of the Roper resonance.

A. Contribution of the $3q^*$ component

The contribution of the $3q^*$ component to the hadronic current of the Roper electroproduction is generally given as

$$J^\mu = \langle R|j_q^\mu|N\rangle \doteq \langle R, \mathbf{p}', S_z', T_z'|j_q^\mu|N, \mathbf{p}, S_z, T_z\rangle. \quad (10)$$

The current j_q^μ is derived by starting from the vector-meson absorption amplitudes described in the $^3P_0$ model

$$T_{V+N\to R}^{q(\lambda)} = 3_{nr}\langle R, \mathbf{0}, S_z', T_z'|V_q^{\text{eff}}|N, -\mathbf{q}, S_z, T_z\rangle \times |V, \mathbf{q}, \lambda_V, t_V\rangle_{nr} \quad (11)$$

[see Appendix B for details] and use of the VMD mechanism in the photon-quark coupling:

$$e\boldsymbol{\epsilon}_\mu^{(\lambda)} J^\mu = \frac{e}{2}\sum_{V=\rho,\omega} \frac{\mathcal{M}_{V+N\to R}^{q(\lambda)}}{g_{VNN}} \frac{M_V^2}{Q^2 + M_V^2}. \quad (12)$$

The vector-meson-nucleon coupling constant g_{VNN} is calculated in the $^3P_0$ model [see Appendix B] and we use $\mathcal{M}_{V+N\to R}^{q(\lambda)} = 2m_M\sqrt{2M_V}T_{V+N\to R}^{q(\lambda)}$ by taking into account a noncovariant normalization (5) in Eq. (11). M_V is the vector-meson mass approximated as $M_V = M_\rho \approx M_\omega$; $\mathbf{p}$, S_z, T_z ($\mathbf{p}', S_z', T_z'$) and $\mathbf{q}, \lambda_\rho, t_\rho$ are the 3-momentum, spin, and isospin projections of the nucleon (the Roper) and of the vector meson, respectively. For convenience we choose the photon momentum as $q^\mu = (q_0, 0, 0, |\mathbf{q}|)$.

After substitution of the quark substructure (see Appendix A 2) for $|N\rangle$, $|R\rangle$, and $|V\rangle$ into Eqs. (10)–(12) and with a simple algebra (here we use $m_q = m_N/3$ for the quark mass), the current matrix element is deduced in the form

$$J^\mu \epsilon_\mu^{(\lambda)} = \frac{\sqrt{3}}{2}\left[\frac{n(y_o)}{n(y)}\right]^{3/2} e^{-\zeta(y)\mathbf{q}^2 b^2/6} \frac{M_V^2}{Q^2 + M_V^2}$$
$$\times \left\{\left\langle\frac{1+\tau_z}{2}\right\rangle_T \delta_{S_z', S_z}\left[\left(\epsilon_0^{(\lambda)} + \frac{\mathbf{q}\cdot\boldsymbol{\epsilon}^{(\lambda)}}{2m_N n(y)}\right)p_2(y, \mathbf{q}^2)\right.\right.$$
$$\left.+ p_0(y)\frac{\mathbf{q}\cdot\boldsymbol{\epsilon}^{(\lambda)}}{2m_N n(y)}\right] - \left\langle\frac{1+5\tau_z}{2}\right\rangle_T$$
$$\times \left.\left\langle\frac{i[\boldsymbol{\sigma}\times\mathbf{q}]\cdot\boldsymbol{\epsilon}^{(\lambda)}}{2m_N}\right\rangle_S p_2(y, \mathbf{q}^2)\right\}. \quad (13)$$

We use the notation

$$\langle\cdots\rangle_S = \langle\tfrac{1}{2}S_z'|\cdots|\tfrac{1}{2}S_z\rangle, \qquad \langle\cdots\rangle_T = \langle\tfrac{1}{2}T_z'|\cdots|\tfrac{1}{2}T_z\rangle,$$

for the spin and isospin matrix elements, respectively, $\epsilon^{(\lambda)\mu} = \{\epsilon_0^{(\lambda)}, \boldsymbol{\epsilon}^{(\lambda)}\}$ is the photon polarization vector and $n, \zeta, p_{0,2}$ are polynomials in $y = b_V/b$ and $\mathbf{q}^2$:

$$n(y) = 1 + \frac{2}{3}y^2, \quad \zeta(y) = \frac{1+\frac{5}{6}y^2}{n}, \quad p_0(y) = \frac{4}{3}\frac{1+y^2}{n},$$
$$p_2(y, \mathbf{q}^2) = \frac{2}{3}\frac{y^2}{n} - \left(\frac{1+y^2}{n}\right)^2\frac{\mathbf{q}^2 b^2}{9}. \quad (14)$$

The transverse ($\lambda = \pm 1$) and longitudinal ($\lambda = 0$) helicity amplitudes for electroproduction of the Roper resonance on the proton ($T_z = 1/2$) are defined by the matrix elements (13) for $\lambda = +1$ and 0 respectively [10,12,19]

$$A_{1/2} = \sqrt{\frac{2\pi\alpha}{q_R}}\left\langle R, \mathbf{0}, +\frac{1}{2}\left| j_q^\mu \epsilon_\mu^{(+)}\right| N, -\mathbf{q}, -\frac{1}{2}\right\rangle,$$
$$S_{1/2} = \sqrt{\frac{2\pi\alpha}{q_R}}\left\langle R, \mathbf{0}, +\frac{1}{2}\left| j_q^\mu \epsilon_\mu^{(0)}\right| N, -\mathbf{q}, +\frac{1}{2}\right\rangle\frac{|\mathbf{q}|}{Q}, \quad (15)$$

where $\alpha = 1/137$ is the fine-structure constant. We introduce

$$q_R = \frac{m_R^2 - m_N^2}{2m_R} \quad (16)$$

for the threshold value of the photon 3-momentum for Roper electroproduction.

In the rest frame of the Roper resonance (the c.m. frame of γ^*N collision) the absolute value of the transferred 3-momentum $\mathbf{q}$ in Eqs. (15) is defined by

$$\mathbf{q}^2 = Q^2 + \left(\frac{Q^2 + m_N^2 - m_R^2}{2m_R}\right)^2. \quad (17)$$

Note that in the region of $0.5 \lesssim Q^2 \lesssim 1.5$ GeV^2 the c.m. frame is very close to the Breit frame, i.e., $Q^2 \approx \mathbf{q}^2$, which is very convenient for comparison of our $\mathbf{q}^2$-dependent results with the relativistic Q^2-dependent ones (substitution of $\mathbf{q}^2 \to Q^2$ does not really change our results if one considers the region $0.5 \lesssim Q^2 \lesssim 1.5$ GeV^2).

We have several remarks regarding current conservation connected to the gauge symmetry of theory. The current conservation condition $q_\mu J^\mu = 0$ for the matrix elements

(10) is not automatically satisfied for the VMD amplitudes. To provide $q_\mu J^\mu = 0$ for a transition current in the VMD amplitudes one needs the conservation of the neutral vector-meson currents $\partial^\mu J_\mu^V = 0$ [44]. In our model these currents J_μ^V are expressed via the amplitudes (11) for which the relation $J^0 = \frac{|\mathbf{q}|}{q_0} J^3$ is not exactly satisfied.

One can try to construct the electromagnetic current using the transverse projector $g_\perp^{\mu\nu} = g^{\mu\nu} + \frac{q^\mu q^\nu}{Q^2}$. This projector does not change the $A_{1/2}$ amplitude, but could lead to some corrections for the components J^0 and J^3. However, the expression for $S_{1/2}$ in Eq. (15) is invariant with respect to such corrections because of the contraction of the current matrix elements with the longitudinal polarization vector

$$\epsilon^{(0)\mu} = \left\{ \frac{|\mathbf{q}|}{Q}, 0, 0, \frac{q_0}{Q} \right\}. \tag{18}$$

Some problem appears in a small region near the photon point with $Q^2 = 0$ where the last factor for $S_{1/2}$ in expression (15) shows singular behavior. In this region we use the following trick. We start from the exact equality

$$J^0 = J^3 \quad \text{at } Q^2 = 0 \tag{19}$$

which follows from the Ward identity at the photon point where $q^0 = |\mathbf{q}|$. Note that at $Q^2 = 0$ we really have $J^0 \approx J^3$ if we use the realistic parameters of the CQM for the wave functions of baryons and mesons. Thus, it is not difficult to transform the approximate equality $J^0 \approx J^3$ to the exact one of Eq. (19) by slightly varying one of the free parameters of the CQM (e.g. the radius b_R of the quark core of the Roper resonance which is not strictly fixed otherwise). The constraint (19) imposed on the parameters of the quark wave functions in the $^3P_0$ amplitudes only stabilizes the behavior of $S_{1/2}$ near the photon point $Q^2 \lesssim$ 0.2–0.3 GeV^2 and does not give pronounced effects for $S_{1/2}$ in the remaining region for Q^2, where $\frac{|\mathbf{q}|}{Q} \approx 1$.

Our results for the helicity amplitudes are

$$A_{1/2} = -\sqrt{\frac{2\pi\alpha}{q_R}} \frac{\sqrt{3}}{2} \mu_p \langle \sigma_+ \rangle \left[\frac{y_R n(y_0)}{N(y, y_R)} \right]^{3/2}$$

$$\times \frac{M_V^2}{Q^2 + M_V^2} e^{-\tilde{\zeta}(y,y_R)(\mathbf{q}^2 b^2)/6} \frac{|\mathbf{q}|}{2m_N} P_2(y, y_R, \mathbf{q}^2) \tag{20}$$

and

$$S_{1/2} = -\sqrt{\frac{2\pi\alpha}{q_R}} \frac{\sqrt{3}}{2} \left[\frac{y_R n(y_0)}{N(y, y_R)} \right]^{3/2} \frac{M_V^2}{Q^2 + M_V^2} e^{-\tilde{\zeta}(y,y_R)\mathbf{q}^2 b^2/6}$$

$$\times \frac{\mathbf{q}^2}{Q^2} \left\{ \left[1 + \frac{q_0(\frac{3}{2}y_R^2 - \frac{1}{2})}{2m_N N(y, y_R)} \right] P_2(y, y_R, \mathbf{q}^2) \right.$$

$$\left. + \frac{q_0}{2m_N N(y, y_R)} P_0(y, y_R) \right\}, \tag{21}$$

where $y \equiv y(Q^2) = y_0 \exp(-Q^2/\chi^2)$. We also take into account a possible difference of the R-resonance radius b_R and the one of the nucleon, which is b, by introducing the ratio $y_R = b_R/b$ which does not depend on Q^2. As a result the polynomials (14) become y_R-dependent N, $P_{0,2}$, $\tilde{\zeta}$ [see Eqs. (B17) and (B18) in Appendix B] and only for $y_R = 1$ they are identical with n, $p_{0,2}$, ζ:

$$n(y) = N(y, y_R = 1), \qquad p_2(y, \mathbf{q}^2) = P_2(y, y_R = 1, \mathbf{q}^2),$$

$$p_0(y) = P_0(y, y_R = 1), \qquad \zeta(y) = \tilde{\zeta}(y, y_R = 1). \tag{22}$$

The vector-meson contribution to the amplitude at high Q^2 should also contain contributions of vector mesons of higher mass $M_V \gtrsim 2M_\rho$. Following the work [30] we use the approximation

$$\frac{M_V^2}{Q^2 + M_V^2} = x \frac{M_\rho^2}{Q^2 + M_\rho^2} + (1 - x) \frac{4M_\rho^2}{Q^2 + 4M_\rho^2}, \quad x = 0.7, \tag{23}$$

which we have checked in the description of the nucleon magnetic form factor.

Note the matrix element (10) for the diagonal transition $N + \gamma^* \rightarrow N$ has the same form as Eq. (13) excluding the algebraic factor $\frac{\sqrt{3}}{2}$ and the polynomial p_2 which should be changed to 1. In the static limit $|\mathbf{q}|, q_0 \rightarrow 0$ this expression defines the charge and the magnetic moment of the nucleon (for $m_q = m_N/3$)

$$\hat{e} = e \frac{I + \tau_z}{2}, \quad \hat{\mu} = \mu_N \frac{I + 5\tau_z}{2}, \quad \mu_N = \frac{e}{2m_N}. \tag{24}$$

The values of μ_p and μ_n are reproduced with an accuracy of about 10%. Moreover, at low and moderate values of Q^2 this amplitude describes the nucleon magnetic form factor G_M with a reasonable accuracy (see Fig. 4). Such an
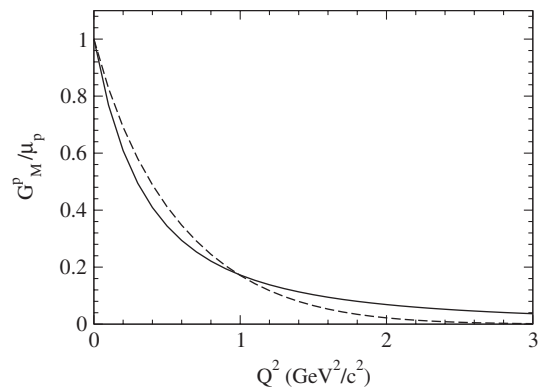

FIG. 4. Normalized magnetic form factor of the proton G_M^p/μ_p in the modified $^3P_0$ model with a Q^2-dependent vector-meson radius and the VMD approach to the $qq\gamma$ interaction (dashed line). Here we use the same set of parameters as in the $N \rightarrow R$ vertex of Fig. 6(a). For comparison, the dipole approximation is also shown (solid line).

accuracy is sufficient (at least in the region $Q^2 \lesssim$ 1–1.5 GeV^2) for the present calculation of the Roper electroproduction amplitudes.

For the nondiagonal process $N + \gamma^* \rightarrow R$ the matrix element (13) defines "the transition magnetic moment" in the limit $|\mathbf{q}|, q_0 \rightarrow q_R$ (i.e. at the photon point):

$$\hat{\mu}_{N \rightarrow R} = -\frac{e}{2m_N} \frac{(I + 5\tau_z)}{2} \frac{\sqrt{3}}{2} \exp[-\zeta(y_0)\mathbf{q}_R^2 b^2/6]$$
$$\times \left[\frac{2y_0^2/3}{1 + 2y_0^2/3} - \left(\frac{1 + y_0^2}{1 + 2y_0^2/3} \right)^2 \frac{\mathbf{q}_R^2 b^2}{9} \right]. \quad (25)$$

The quantity $\hat{\mu}_{N \rightarrow R}$ gives the value (apart from a kinematical factor $\langle \sigma_+ \rangle \sqrt{q_R/2}$) of the transverse helicity amplitude $A_{1/2}$ at the photon point. The first term in the square brackets of the right-hand side of Eq. (25)

$$Z_V = \frac{2y_0^2/3}{1 + 2y_0^2/3}, \qquad y_0 = b_V/b \quad (26)$$

[or the first term of the polynomial p_2 in Eq. (14)] is present because of the nonlocality of the Vqq interaction defined by Eq. (11). There the operator V_q^{eff} leads to an insertion of the inner $\bar{q}q$ wave function of the vector meson into the Vqq vertex.

The size of the nonlocal region is defined by the spatial scale of the meson wave function. For a pointlike vector meson ($b_V = 0$) the value of Z_V reduces to zero, and the matrix element for the transition $N + \gamma_T^* \rightarrow R$ reduces to the matrix element of the EEM with a local Vqq vertex. The EEM matrix element vanishes in the limit $|\mathbf{q}| \rightarrow 0$, as it should because of the orthogonality of the spatial parts of the wave functions of N and R.

Such behavior of the $A_{1/2}$ amplitude near the photon point $Q^2 = 0$ is characteristic of all the models which start from local γqq or Vqq vertices at high Q^2 and continue to use such interaction in the soft region of small $Q^2 \lesssim 6/b_V^2$, where the electromagnetic interaction is modified by the inner structure of vector mesons as $\bar{q}q$ bound states.

As a result, in models with a local operator for the γqq (or Vqq) interaction (see, e.g., the relativistic models [10–12,19,45]) the transverse helicity amplitude $A_{1/2}$ vanishes in the limit $Q^2 \rightarrow 0$ [or it approaches a small value which is defined by the second term in the last line of Eq. (25) modified by relativistic corrections].

The importance of the nonlocality of the Vqq interaction in the description of Roper electroproduction near the photon point was first noted by the authors of the $^3P_0$ model [7]. In Ref. [15] this nonlocal $^3P_0$ interaction was used for the calculation of the helicity amplitudes on the basis of a dynamical quark model of baryons. Unfortunately, the authors of [15] have only used a trivial sum of $^3P_0$ and EEM interaction terms (a "generalized EEM"). With this ansatz they describe both the low- and high-Q^2 amplitudes with a common mechanism, and the same quark dynamics was used for both the nucleon and the Roper resonance.

Now it becomes evident that intermediate meson-baryon states ("hadron loops") can play a considerable role in the quark dynamics of excited baryons, and such meson-baryon states should be taken into account (see, e.g., Ref. [46,47]). Since the resonance pole of the Roper [2] 1365–i95 MeV is rather close to the $N + \sigma$ threshold the intermediate $N + \sigma$ configuration will play a more important role in the inner dynamics of the Roper as compared, for example, to the case of the nucleon.

In our opinion, a first step in the study of the nontrivial inner structure of the Roper resonance could be an evaluation on the basis of the recent CLAS data [5], where a nonvanishing probability for a possible $N + \sigma$ component of the Roper is compatible with the data.

B. Contribution of the hadronic $N + \sigma$ component

The hadronic $N\sigma$ loop diagrams contributing to the Roper electroexcitation are shown in Fig. 3. The $RN\sigma$ vertex is defined by the nonlocal Lagrangian $\mathcal{L}_R$ of Eq. (8). For the $NN\sigma$ vertex we use a similar nonlocal Lagrangian with the correlation function $\Phi_N(y^2)$,

$$\mathcal{L}_N = g_{NN\sigma}\sigma(x)\int dy \Phi_N(y^2)\bar{N}(x + y/2)N(x - y/2), \quad (27)$$

where $g_{NN\sigma}$ is the $NN\sigma$ coupling constant; $\tilde{\Phi}_N(-k_E^2) = \exp(-\frac{k_E^2}{\Lambda_N^2})$ is the Fourier transform of $\Phi_N(y^2)$ in Euclidean space with $\Lambda_N = 0.7$–1 GeV.

The electromagnetic interaction Lagrangian contains two pieces

$$\mathcal{L}_{\text{int}}^{\text{em}} = \mathcal{L}_{\text{int}}^{\text{em}(1)} + \mathcal{L}_{\text{int}}^{\text{em}(2)}, \quad (28)$$

which are generated after the inclusion of photons. The first term $\mathcal{L}_{\text{int}}^{\text{em}(1)}$ is standard and is obtained by minimal substitution in the free Lagrangian of the proton and charged Roper resonance:

$$\partial^\mu B \rightarrow (\partial^\mu - ie_B A^\mu)B, \quad (29)$$

where B stands for p, R^+ and e_B is the electric charge of the field B. The interaction Lagrangian $\mathcal{L}_{\text{int}}^{\text{em}(1)}$ reads

$$\mathcal{L}_{\text{int}}^{\text{em}(1)}(x) = e_B \bar{B}(x) A\!\!\!/ B(x). \quad (30)$$

The second electromagnetic interaction term $\mathcal{L}_{\text{int}}^{\text{em}(2)}$ is generated when the nonlocal Lagrangians (8) and (27) are gauged. The gauging proceeds in a way suggested and extensively used in Refs. [43,48,49]. In order to guarantee local $U(1)$ gauge invariance of the strong interaction Lagrangian one multiplies each charged field in (8) and (27) with a gauge field exponential $e^{-ie_B I(y,x,P)}$. The exponent contains the term

$$I(y, x, P) = \int_x^y dz_\mu A^\mu(z), \qquad (31)$$

where P is the path of integration from x to y. Then we obtain

$$\mathcal{L}_R^{\text{str+em}(2)}(x) = g_{R\sigma N}\bar{R}^0(x) \int dy \Phi_R(y^2) n(x + w_{\sigma N}y)$$

$$\times \sigma(x - w_{N\sigma}y) + g_{R\sigma N}\bar{R}^+(x) \int dy \Phi_R(y^2) e^{-ie_p I(x+w_{\sigma N}y, x, P)}$$

$$\times p(x + w_{\sigma N}y)\sigma(x - w_{N\sigma}y) + \text{H.c.} \qquad (32)$$

and

$$\mathcal{L}_N^{\text{str+em}(2)}(x) = g_{NN\sigma}\sigma(x) \int dy \Phi_N(y^2)\left(\bar{n}\left(x + \frac{y}{2}\right)n\left(x - \frac{y}{2}\right)\right.$$

$$\left. + \bar{p}\left(x + \frac{y}{2}\right)e^{-ie_p I(x-(y/2), x+(y/2), P)}p\left(x - \frac{y}{2}\right)\right). \qquad (33)$$

An expansion of the gauge exponential up to terms linear in A^μ leads to $\mathcal{L}_{\text{int}}^{\text{em}(2)}$.

The full Lagrangian consistently generates the required matrix element of the electroexcitation amplitude which is linked to coming the hadronic molecular component of the Roper. Because of gauge invariance the electromagnetic vertex function $\Lambda_\mu(p, p')$ is orthogonal to the photon momentum $q^\mu \Lambda_\mu(p, p') = 0$. As a result, the vertex function $\Lambda_\mu(p, p')$ is given by the sum of the gauge-invariant pieces of the triangle (Δ), the bubble (bub), and the pole (pol) diagrams, while the non gauge-invariant parts of these diagrams cancel in the sum:

$$\Lambda_\mu(p, p') = \Lambda_{\mu,\Delta}^\perp(p, p') + \Lambda_{\mu,\text{bub}}^\perp(p, p') + \Lambda_{\mu,\text{pol}}^\perp(p, p'). \qquad (34)$$

The contribution of each diagram can be split into a gauge-invariant piece and a reminder term, which is not gauge invariant, by introducing the decomposition

$$\gamma_\mu = \gamma_\mu^\perp + q_\mu \frac{\slashed{q}}{q^2}, \qquad p_{i\mu} = p_{i\mu}^\perp + q_\mu \frac{p_i q}{q^2}, \qquad (35)$$

with $\gamma_\mu^\perp q^\mu = 0$, $p_{i\mu}^\perp q^\mu = 0$, where p_i is p or p'. The vertex function $\Lambda_\mu^\perp(p_1, p_2)$ can then be expressed in terms of $\gamma_\mu^\perp$ and $p_{i\mu}^\perp$.

In the case of the triangle diagram of Fig. 3(a) we include the q^2 dependence of the photon-nucleon vertices in correspondence with data. Taking into account the nucleon structure the $e_p \bar{p}\gamma_\perp^\mu p$ vertex is modified as

$$\bar{N}\left(\gamma_\perp^\mu F_1^N(q^2) + i\frac{\sigma^{\mu\nu}q_\nu}{2m_N}F_2^N(q^2)\right)N, \qquad (36)$$

where $F_1^N(q^2)$ and $F_2^N(q^2)$ are the Dirac and Pauli form factors, which are normalized as $F_1^N(0) = e_N$ (nucleon electric charge) and $F_2^N(0) = \kappa_N$ (nucleon anomalous magnetic moment). The form factors $F_{1,2}^N$ are expressed
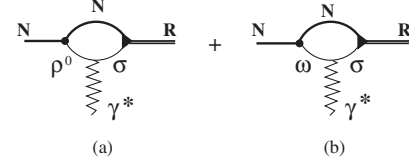

FIG. 5. $\sigma\gamma^* V$ ($V = \rho^0, \omega$) processes in the electroexcitation of the $N\sigma$ bound state.

through the electric and magnetic Sachs form factors G_E^N, G_M^N of the nucleon as $F_1^N = (G_E^N + \tau G_M^N)/(1 + \tau)$, $F_2^N = (G_M^N - G_E^N)/(1 + \tau)$, $\tau = -q^2/4m_N^2$. For the Sachs form factors we use the Kelly parametrization [50]:

$$G(\tau) \propto \frac{\sum_{k=1}^n a_k \tau^k}{1 + \sum_{k=0}^{n+2} b_k \tau^k}. \qquad (37)$$

Two additional contributing diagrams to the electroproduction of the Roper resonance are shown in Fig. 5. The amplitudes of the $\sigma\gamma^* V$ ($V = \rho^0, \omega$) transition are written in the form

$$\frac{e g_{\sigma\gamma V}}{M_V}(g^{\mu\nu}q \cdot k - k^\mu q^\nu), \qquad (38)$$

where k is the vector-meson momentum. The values for the coupling constants $g_{\sigma\gamma V}$ are estimated in the branch ratio model [51] with $g_{\sigma\gamma\rho^0} \simeq 0.25$, $g_{\sigma\gamma\omega} \simeq 0.05$.

The contributions of the amplitudes of Fig. 5 were estimated using the local limit for the $NN\rho$ and $NN\omega$ vertices. We found a very small contribution compared to the diagrams of Fig. 3. Both $\sigma\gamma V$ diagrams are explicitly transverse under contraction with the photon momentum q_μ.

Finally, the helicity amplitudes for the electromagnetic excitation are defined like in (15)

$$A_{1/2} = \sqrt{\frac{2\pi\alpha}{q_R}}\left\langle R, \frac{1}{2} \left| J_+ \right| N, -\frac{1}{2}\right\rangle\xi,$$

$$S_{1/2} = \sqrt{\frac{2\pi\alpha}{q_R}}\left\langle R, \frac{1}{2} \left| J_0 \right| N, \frac{1}{2}\right\rangle\xi,$$

$$J_+ = -\frac{1}{\sqrt{2}}(J_x + iJ_y), \qquad (39)$$

where J^μ is the electromagnetic transition current defined by the diagrams of Fig. 3. The helicity amplitudes (39) are defined up to a phase ξ. The amplitudes are written in the c.m. frame of the nucleon and the photon, i.e., in the Roper resonance rest frame. The 4-spinors present in $|R\rangle$, $|N\rangle$ are normalized as $\bar{R}R = \frac{m_R}{\varepsilon_R}$, $\bar{N}N = \frac{m_N}{\varepsilon_N}$.

IV. RESULTS AND COMPARISON WITH DATA

A. Parameter fitting

In the calculation the helicity amplitudes $A_{1/2}$ and $S_{1/2}$ we use two variants for the free parameters, denoted as (a)

and (b), both typical for the CQM. They were only fitted to the $A_{1/2}$ JLab data [5,6] without any additional adjustment to the $S_{1/2}$ data [we only take into account the condition (19)]. One of the parameter sets gives the best description of the data in the soft region with $0 \lesssim Q^2 \lesssim 1 \, \text{GeV}^2$ and the other one the optimal description in the whole measured interval including the hard region of $Q^2 \gtrsim 1.5\text{–}2 \, \text{GeV}^2/c^2$.

Note, we do not pretend that the nonrelativistic model for the quark configurations is able to describe data for the whole hard region. We only study the compatibility of our predictions with the behavior of the data in the transition region between the soft and the hard regimes (a relativistic generalization of the model could be the next step to start from a hard variant which gives a realistic description of the data at low and moderate values of Q^2).

Our parameters are grouped into two sets: one set of parameters is related to the $3q$ components of the baryons and the other set is connected with the $N\sigma$ molecular component. One of the quark model parameters is fixed by the strong constraints following from the Ward identity [parameter b_R, see Eq. (19)]. The additional free quark parameters b, b_V, and χ are adjusted to optimize the description of the proton magnetic form factor in the considered region of Q^2, including the intermediate values $0.5 \lesssim Q^2 \lesssim 1.5 \, \text{GeV}^2/c^2$, and of the above mentioned subset of data on the helicity amplitude $A_{1/2}$. Two of these fitted parameters, b and b_V, should, in addition, have values which are typical for the quark core radii of the nucleon and a vector meson with $b \approx b_V \approx 0.5$ fm. The third fitted parameter χ should not be smaller than the characteristic scale $\sim (1\text{–}1.5)m_N$ associated with short-range effects in eN scattering. These additional constraints on the parameters b, b_V, and χ sufficiently limit the range of allowed values. Finally, we arrive at the following two optimal sets of quark component parameters:

(a) a hard variant

$$b = 0.48 \, \text{fm}, \qquad y_0 = \frac{b_V}{b} = 0.9,$$

$$\chi^2 = 1.5 m_N^2, \qquad b_R = 0.9444 b, \qquad (40)$$

adjusted to the data of $A_{1/2}$ with taking into account the hard region of $Q^2 \gtrsim 1.5\text{–}2 \, \text{GeV}^2/c^2$ and

(b) a soft variant

$$b = 0.54 \, \text{fm}, \qquad y_0 = \frac{b_V}{b} = 0.81,$$

$$\chi^2 = 4 m_N^2, \qquad b_R = 0.8824 b, \qquad (41)$$

fitted to the $A_{1/2}$ data with $0 \lesssim Q^2 \lesssim 1 \, \text{GeV}^2/c^2$.

The set of parameters related to the molecular component includes the mixing parameter θ, the scale parameters Λ_M, Λ_N and the parameter λ entering in the vertex function of the Roper. Further parameters linked to the σ are the mass M_σ, the width Γ_σ, and the strong coupling constant

$g_{\sigma NN}$. The parameters $\Lambda_M \approx \Lambda_N \approx 1$ GeV are approximately taken at the scale set by the light baryons. The parameter λ is fixed through the orthogonality condition $\langle R|N \rangle = 0$ (finally fitted at $\lambda = 2.45$). For the σ resonance we take values which are reasonable [2] [a wide range of values is given by $M_\sigma = (0.4 - 1.2)$ GeV, $\Gamma_\sigma = (0.5 - 1)$ GeV, and $g_{\sigma NN} \approx 5\text{–}10$]. Some fine-tuning of these parameters to the complete range of data on $A_{1/2}$ results in the following set of molecular parameters:

$$\Lambda_M = 1 \, \text{GeV}, \quad \Lambda_N = 0.8 \, \text{GeV}, \quad M_\sigma = 0.5 \pm 0.05 \, \text{GeV},$$

$$\Gamma_\sigma = 0.75 \pm 0.25 \, \text{GeV}, \quad g_{\sigma NN} = 5. \qquad (42)$$

The mixing parameter θ is fixed in the low-energy region ($0 \lesssim Q^2 \lesssim 1 \, \text{GeV}^2/c^2$) of $A_{1/2}$, where the molecular component is optimized to reproduce the difference between the $3q$ contribution and the JLab data. We obtain $\sin\theta = 0.6$ and 0.7 for sets (a) and (b), respectively. The complete results for the parameters should be considered preliminary and be tested seriously in further applications.

It is important to remark that in the evaluation of the helicity amplitudes we use the free σ meson propagator (as some kind of approximation), while in case of the strong Roper decay $R \rightarrow N + 2\pi$ we had to use the Breit-Wigner σ-meson propagator. The sensitivity of the results to a variation of the σ meson mass from 0.45 to 0.55 GeV gives a variation of the helicity amplitudes up to 10%. The sensitivity of the strong decay $\Gamma(R \rightarrow N + 2\pi)$ to a variation of Γ_σ is discussed in Sec. IV C. In fact, more precise data on $\Gamma(R \rightarrow N + 2\pi)$ can give a new, additional constraint on Γ_σ.

B. Helicity amplitudes

The calculated helicity amplitudes $A_{1/2}$ and $S_{1/2}$ are shown in Figs. 6(a) and 6(b) [using the parameter sets (a) and (b), respectively]. We also show separately the contributions to the amplitude from the quark and the hadron molecule components (dashed and dashed-dotted curves, respectively). The comparison with the standard $^3P_0$ model calculation with a fixed value for the vector-meson radius $b_V = 0.9b$ (dotted curves) demonstrates the following: a smooth transition from the $^3P_0$ γRN vertex [Fig. 1(a)] to the partonlike one [Fig. 1(b)] using a Q^2-dependent vector-meson radius $b_V(Q^2) \rightarrow 0$ leads to considerable improvement of the standard $^3P_0$ model results at moderate values of Q^2.

The quark core component of R plays the main role in the electroproduction of the Roper resonance for this Q^2 region ($Q^2 \gtrsim 1\text{–}1.5 \, \text{GeV}^2/c^2$). For small values of $Q^2 \lesssim 1 \, \text{GeV}^2$, where the contribution of the meson cloud should also be important, it can be effectively taken into account in the framework of $^3P_0$ and VMD models. However, such a model overestimates the transverse amplitude $A_{1/2}$ in the region $0.5 \lesssim Q^2 \lesssim 1 \, \text{GeV}^2$ (the dashed line in Fig. 6). The description of the JLab data [5,6] on $A_{1/2}$ can be

considerably improved if one takes a combined structure for the Roper in the form of $|R\rangle = \cos\theta|3q^*\rangle + \sin\theta|N + \sigma\rangle$. The adjustable parameter θ fitted to the JLab data in this region is about $\cos\theta = 0.8$ [for the hard variant (a)] or $\cos\theta = 0.7$ [for set (b)], in both cases indicating an admixture of $N\sigma$ component of about 50%.

The hard version (a) looks more plausible in the description of both amplitudes $A_{1/2}$ and $S_{1/2}$, while set (b) only represents a fit to the soft-Q^2 (up to $Q^2 \approx 1$ GeV^2/c^2) behavior of the transverse amplitude $A_{1/2}$. In the soft-Q^2 region the contribution of the pion cloud and the influence of the coupled channel $\Delta + \pi$ are important [6,20–23]. Both effects should be taken into account in further detailed calculations.

C. Decay widths

When the weight of the $N + \sigma$ component in the Roper resonance in terms of $\sim\sin^2\theta$ is fixed, the Roper decay width for the transition $N + (\pi\pi)_{S\,\mathrm{wave}}^{I=0}$ can be calculated. The assumption that the quark part of the Roper just gives a

very small contribution through a virtual transition $R \to N + \sigma$ is justified in our quark model [see, e.g., our evaluation of the quark amplitude $\mathcal{M}_{R\to N+\sigma}^q$ in Eq. (B20) which goes to zero at $y_\sigma = 1$ as it follows from Eq. (B22)]. Then the transition is described as the virtual decay of the molecular part to $N + \sigma$ followed by the $\sigma \to \pi\pi$ decay. The diagram for such a mechanism is shown in Fig. 7.

The probability $|M_{fi}|^2$ for the transition process of Fig. 7 contains the Breit-Wigner representation for the intermediate σ-meson state with

$$|M_{fi}|^2 = g_{R\sigma N}^2 g_{\sigma\pi\pi}^2 \tilde{\Phi}_R^2(k^2) \frac{(m_N + m_R)^2 - s_{\pi\pi}}{(m_\sigma^2 - s_{\pi\pi})^2 + m_\sigma^2\Gamma_\sigma^2(s_{\pi\pi})},$$

$$\Gamma_\sigma(x) = \Gamma_\sigma \frac{m_\sigma}{\sqrt{x}} \frac{\sqrt{x - 4m_\pi^2}}{\sqrt{m_\sigma^2 - 4m_\pi^2}}, \qquad x = s_{\pi\pi} \equiv k_\sigma^2, \quad (43)$$

where $k = p_R - \omega_{N\sigma} p_N$ and the coupling constant $g_{\sigma\pi\pi}$ is deduced from the two-pion decay width of the σ with $g_{\sigma\pi\pi}^2 = \frac{32\pi}{3}\Gamma_\sigma m_\sigma (1 - \frac{4m_\pi^2}{m_\sigma^2})^{-1/2}$. The coupling constant
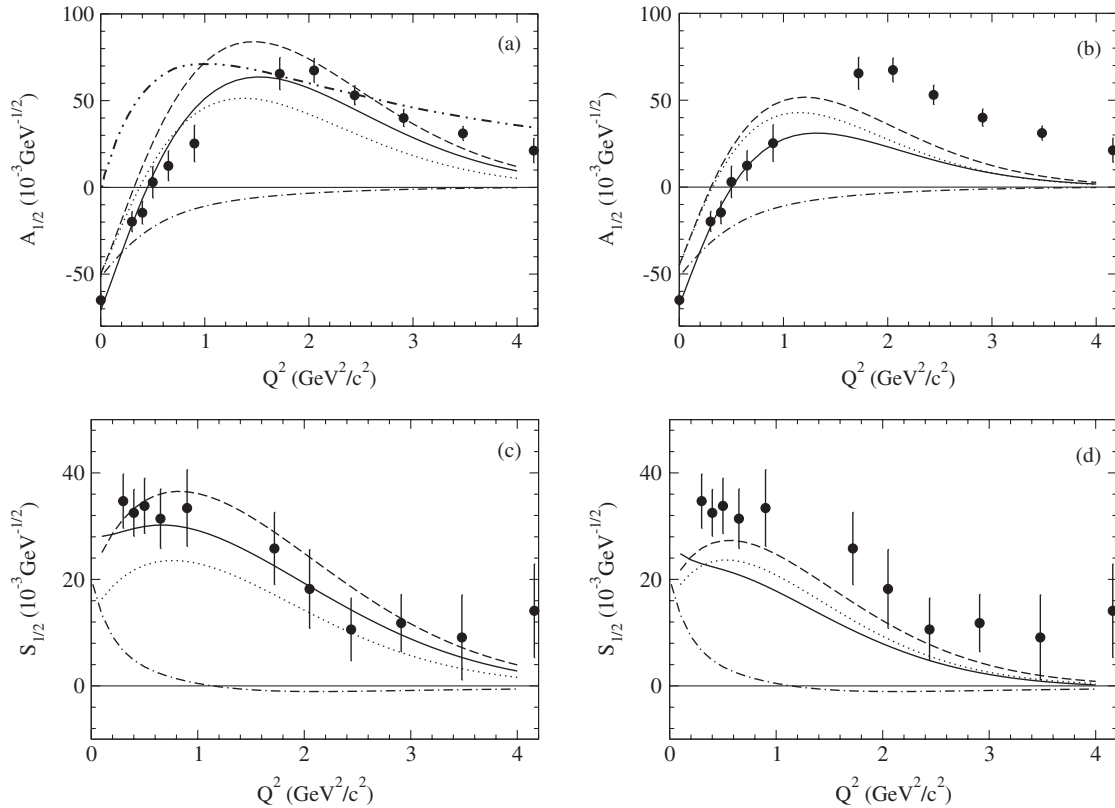

FIG. 6. Helicity amplitudes $A_{1/2}$ (top panels) and $S_{1/2}$ (bottom) for two variants of the model parameters, hard (left panels) and soft (right panels), in comparison to JLab data [5,6]. Dotted curves: the quark core excitation amplitudes $|3q\rangle + \gamma^* \to |3q^*\rangle$ calculated in the framework of the standard $^3P_0$ + VMD model with a fixed vector-meson radius $b_V = y_0 b$. Dashed curves: the same amplitudes calculated in a modified $^3P_0$ + VMD model with a Q^2-dependent scale parameter $y = y_0 e^{-Q^2/x^2}$ for the vector-meson radius $b_V = yb$. Dashed-dotted curves: helicity amplitudes for the electroexcitation of the hadron molecule $N + \sigma$. Solid curves: the full calculation of $A_{1/2}$ and $S_{1/2}$ in terms of a combined structure $R = \cos\theta|3q^*\rangle + \sin\theta|N + \sigma\rangle$. For comparison, the valence quark contribution to $A_{1/2}$ calculated in Ref. [19] on the basis of a covariant spectator model is also shown (the dashed-double-dotted curve in the left top panel).
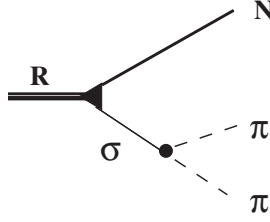
FIG. 7. $R \to N + (\pi + \pi)_{I=0}$ decay process via the σ-meson resonance.

$g_{R\sigma N}$ of the hadron-molecular vertex is defined by the compositeness condition (7).

The result for the $R \to N + (\pi\pi)_{S\,\text{wave}}^{I=0}$ decay width is presented by an integral over the variables of the phase space volume

$$\Gamma_{R \to N\sigma(\pi\pi)} = \frac{3\sin^2\theta}{512\pi^3 m_R^3}$$
$$\times \int_{4m_\pi^2}^{(m_R - m_N)^2} \frac{ds_{\pi\pi}}{s_{\pi\pi}} |M_{fi}|^2 \lambda^{1/2}(m_R^2, m_N^2, s_{\pi\pi})$$
$$\times \lambda^{1/2}(s_{\pi\pi}, m_\pi^2, m_\pi^2), \tag{44}$$

with $\lambda(a, b, c) = a^2 + b^2 + c^2 - 2ab - 2bc - 2ac$.

The numerical value for $\Gamma_{R \to N\sigma}$ with $g_{R\sigma N} = 6.39$ [fixed by the compositeness condition (7)] and a molecular admixture in the Roper of $\sin\theta \simeq 0.6$ is

$$\Gamma_{R \to N\sigma(\pi\pi)} = (19.0\text{–}26.7) \text{ MeV}, \tag{45}$$

where the lower and upper limits correspond to a variation of the σ decay width Γ_σ from 0.5 to 1 GeV, respectively, (the variation of the σ-meson mass $M_\sigma = 500 \pm 50$ MeV can only change the result within 10%). This should be compared to the PDG [2] value $\Gamma_{R \to N\sigma(\pi\pi)} \approx (0.05\text{–}0.1)$ $\Gamma_R^{\text{tot}}(\approx 15\text{–}30 \text{ MeV}))$ or the recent data [3] $\Gamma_{R \to N\sigma} = 71 \pm 17$ MeV. It is clear that the strong Roper decay can serve as a constraint on Γ_σ, however present results for $\Gamma_{R \to N\sigma(\pi\pi)}$ are compatible with all values of Γ_σ.

The pion decay width calculated for the quark part of the Roper resonance in the framework of our approach $(\Gamma_{R \to \pi N}^q \simeq 36$ MeV) is not as small as in the case of EEM evaluations $(\Gamma_{R \to \pi N}^{\text{EEM}} \simeq 4$ MeV) but it is still several times smaller than the PDG value of $\Gamma_{R \to N+\pi} \approx (0.55\text{–}0.75)\Gamma_R^{\text{tot}}$. It is clear that considerable corrections to $\Gamma_{R \to \pi N}^q$ can come from the pion cloud contribution which is neglected here.

V. CONCLUSIONS

We suggested a two-component model of the lightest nucleon resonance $R = N_{1/2^+}(1440)$ as a combined state of the quark configuration $sp^2[3]_X$ and the hadron molecule component $N + \sigma$. This approach allows us to describe with reasonable accuracy the recent CLAS electroproduction data [5,6] at low and moderate values

of Q^2 with $0 \leq Q^2 \lesssim 1.5\text{–}2$ GeV^2. In the model the $R \to N + (\pi\pi)_{S\,\text{wave}}^{I=0}$ transition process is interpreted as the decay of a virtual σ meson in the $N + \sigma$ component. The calculated decay width $\Gamma_{R \to N\sigma(\pi\pi)}$ correlates well with the PDG value [2] and the recent CB-ELSA and A2-TAPS data [3].

The weight of the $N + \sigma$ component in the Roper with $\sin^2\theta \approx 0.36$ is compatible with the CLAS data at low and moderate Q^2. This weight is also compatible with the value of the helicity amplitude $A_{1/2}$ at the photon point and with the data on the $R \to N + (\pi\pi)_{S\,\text{wave}}^{I=0}$ decay width.

However, our evaluations have shown that at low Q^2 the contribution of the pion cloud to the amplitude $A_{1/2}$ can be considerable. For example, this is evident from Fig. 6(a), where the discrepancy of our results and the CLAS data is about 1–1.5 experimental error bars. Still, this discrepancy is considerably smaller than in the case of previous quark models: note the predictions of the valence quark covariant spectator model (the dashed-double-dotted curve in Fig. 6(a) adapted from Ref. [19]) or predictions of the LF models in the same region of $Q^2 \lesssim 1$ GeV^2/c^2.

In this paper we tried to show that the description of transition amplitudes in terms of partonlike models, which are very good at high Q^2, can be naturally transformed into a description in terms of the soft vector-meson cloud. This smooth transition is achieved by ''switching on'' a nonzero radius of the intermediate vector meson. The vector-meson V of finite size generates a nonlocal Vqq interaction. This weakens the effect of the orthogonality of the spatial R and N wave functions in the transition matrix element $N + \gamma_T^* \to R$, and the amplitude $A_{1/2}$. Resulting theoretical values, which match the data, are contrary to the standard predictions of LF models, which lead to nonzero and (negative) large values at the photon point.

Further we plan to develop a relativistic version of the suggested electroexcitation mechanism.

APPENDIX A: HADRON QUARK WAVE FUNCTIONS

1. Basic elements

We use the standard definitions for the harmonic oscillator wave functions

$$\varphi_{0S}(\mathbf{p}, r_0) = (4\pi r_0^2)^{3/4} e^{-p^2 r_0^2/2},$$

$$\varphi_{2S}(\mathbf{p}, r_0) = \sqrt{\frac{3}{2}}\left(1 - \frac{2}{3} p^2 r_0^2\right)\varphi_{0S}(\mathbf{p}, r_0),$$

$$\varphi_{1P,m}(\mathbf{p}, r_0) = \sqrt{\frac{2}{3}}p r_0 \varphi_{0S}(\mathbf{p}, r_0)\sqrt{4\pi}Y_{1m}(\hat{\mathbf{p}}). \tag{A1}$$

The relative momenta in the quark (antiquark) systems with numbering $i = 1, 2, 3, 4, 5$ (see Figs. 1 and 8) are set up as

$$\varkappa_1 = \tfrac{1}{2}(\mathbf{p}_1 - \mathbf{p}_2), \qquad \varkappa_2 = \tfrac{1}{3}(\mathbf{p}_1 + \mathbf{p}_2) - \tfrac{2}{3}\mathbf{p}_4,$$

$$\varkappa_2' = \tfrac{1}{3}(\mathbf{p}_1 + \mathbf{p}_2) - \tfrac{2}{3}\mathbf{p}_3, \qquad \varkappa_M = \tfrac{1}{2}(\mathbf{p}_3 - \mathbf{p}_5),$$

$$\mathbf{p}_M = \mathbf{p}_3 + \mathbf{p}_5. \tag{A2}$$

In the rest frame with $\mathbf{P}'_{R(N)} = \mathbf{p}_1 + \mathbf{p}_2 + \mathbf{p}_3 = 0$ we have the relations

$$\mathbf{p}_M = \mathbf{k}, \qquad \mathbf{P}_N = \mathbf{p}_1 + \mathbf{p}_2 + \mathbf{p}_4 = -\mathbf{k},$$

$$\mathbf{p}_4 - \mathbf{p}_3 = -\mathbf{k}, \qquad \varkappa_M = -\varkappa_2' - \frac{\mathbf{k}}{2},$$

$$\mathbf{p}_4 + \mathbf{p}_3 = -2\varkappa_2' - \mathbf{k}, \tag{A3}$$

which are used with $m_1 = m_2 = m_3 = m_q = m_N/3$ and

$$\nu_1 = 2, \qquad \nu_2 = \frac{3}{2}, \qquad m_{12} = \frac{m_1 m_2}{m_1 + m_2} = \frac{m_q}{\nu_1},$$

$$m_{(12)3} = \frac{(m_1 + m_2)m_3}{m_1 + m_2 + m_3} = \frac{m_q}{\nu_2}, \tag{A4}$$

in the calculation of matrix elements.

2. Quark configurations

a. Baryons

The translationally invariant quark configurations $s^3[3]_X$ and $sp^2[3]_x$, $L = 0$ are represented in terms of harmonic oscillator wave functions (A1) depending on the relative momenta (A2) as
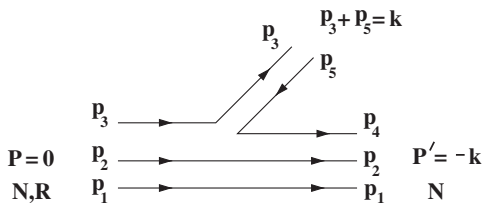

FIG. 8. Quark diagram of the $^3P_0$ model for the meson-baryon coupling.

$$\Psi_N(\varkappa_1\varkappa_2; S_z, T_z) = \varphi_{0S}(\varkappa_1, \sqrt{\nu_1}b)\varphi_{0S}(\varkappa_2, \sqrt{\nu_2}b)\psi_N^{ST}(124), \tag{A5}$$

$$\Psi_R(\varkappa_1, \varkappa_2'; S_z, T_z) = \left[\sqrt{\frac{1}{2}}\varphi_{0S}(\varkappa_1, \sqrt{\nu_1}b)\varphi_{2S}(\varkappa_2', \sqrt{\nu_2}b)\right.$$

$$\left. + \sqrt{\frac{1}{2}}\varphi_{2S}(\varkappa_1, \sqrt{\nu_1}b)\varphi_{0S}(\varkappa_2', \sqrt{\nu_2}b)\right]\psi_N^{ST}(123). \tag{A6}$$

The spin-isospin part ψ_N^{ST} for both configurations is described by the state vector

$$\psi_N^{ST}(124) = \sum_{\mu_4 t_4}\left[\sqrt{\frac{1}{2}}\left(1(S_z - \mu_4)\frac{1}{2}\mu_4\,\Big|\,\frac{1}{2}S_z\right)\right.$$

$$\times \left(1(T_z - t_4)\frac{1}{2}t_4\,\Big|\,\frac{1}{2}T_z\right)|S_{12} = 1, S_z - \mu_4\rangle|T_{12}$$

$$= 1, T_z - t_4\rangle + \sqrt{\frac{1}{2}}\delta_{\mu_4, S_z}\delta_{t_4, T_z}|S_{12} = 0, 0\rangle|$$

$$\times T_{12} = 0, 0\rangle\Big]\chi_{\mu_4}\xi_{t_4}, \tag{A7}$$

where χ_{μ_i} (ξ_{t_i}) is the spinor (isospinor) of i-th quark, μ_i (t_i) is the spin (isospin) projection; $i = 1, 2, 4$ for the nucleon and $i = 1, 2, 3$ for the Roper.

b. Mesons

(1) Pseudoscalar (π) and scalar (σ)

$$\Psi_\pi(\varkappa_\pi, t_\pi) = \varphi_{0S}(\varkappa_\pi, \sqrt{\nu_1}b_\pi)\sum_{\mu_3\mu_5}\left(\frac{1}{2}\mu_3\frac{1}{2}\mu_5|00\right)$$

$$\times \sum_{t_3 t_5}\left(\frac{1}{2}t_3\frac{1}{2}t_5|1t_\pi\right)\chi_{\mu_3}\chi_{\mu_5}\xi_{t_3}\xi_{t_5}, \tag{A8}$$

$$\Psi_\sigma(\varkappa_\sigma) = \varphi_{0S}(\varkappa_\sigma, \sqrt{\nu_1}b_\sigma)\sqrt{\nu_1}b_\sigma\varkappa_\sigma\sqrt{\frac{4\pi}{3}}$$

$$\times \sum_m (1m1 - m|00)\sum_{\mu_3\mu_5}\left(\frac{1}{2}\mu_3\frac{1}{2}\mu_5|1m\right)Y_{1-m}(\hat{\varkappa}_\sigma)$$

$$\times \sum_{t_3 t_5}\left(\frac{1}{2}t_3\frac{1}{2}t_5|00\right)\chi_{\mu_3}\chi_{\mu_5}\xi_{t_3}\xi_{t_5}. \tag{A9}$$

(2) Vectors (ρ, ω)

$$\Psi_\rho(\varkappa_\rho, \lambda_\rho, t_\rho) = \varphi_{0S}(\varkappa_\rho, \sqrt{\nu_1}b_\rho)\sum_{\mu_3\mu_5}\left(\frac{1}{2}\mu_3\frac{1}{2}\mu_5|1\lambda_\rho\right)$$

$$\times \sum_{t_3 t_5}\left(\frac{1}{2}t_3\frac{1}{2}t_5|1t_\rho\right)\chi_{\mu_3}\chi_{\mu_5}\xi_{t_3}\xi_{t_5} \tag{A10}$$

[for the ω use the substitution

$$\left(\frac{1}{2}t_3\frac{1}{2}t_5\Big|1t_\rho\right) \to \left(\frac{1}{2}t_3\frac{1}{2}t_5\Big|00\right) \tag{A11}$$

in Eq. (A10)].

APPENDIX B: MESON-BARYON COUPLING

The meson-baryon vertex generated by the effective pair creation operator $V_{\bar{q}q}^{\text{eff}}$ is schematically sketched in Fig. 8. Performing a recoupling of quark (antiquark) variables in the matrix element $\langle M|\langle N|V_{\bar{q}q}^{\text{eff}}|N(R)\rangle$ ($M = \pi, \sigma, \rho, \omega$), omitting the isospin part and other trivial factors $[\frac{g_q}{2m_q}, \frac{g_q}{2m_q}, \delta(\mathbf{p}_4 + \mathbf{p}_5)$, etc.] we obtain for the nontrivial spin part of the effective πqq and ρqq vertices the following expressions:

$$\pi qq: \boldsymbol{\sigma} \cdot \mathbf{p}_4, \qquad \rho qq: (-\mathbf{p}_4 + i[\boldsymbol{\sigma} \times \mathbf{p}_4]) \cdot \boldsymbol{\epsilon}^{(\lambda_\rho)}, \tag{B1}$$

where

$$\boldsymbol{\epsilon}^{(\lambda_\rho)\mu} = \{\boldsymbol{\epsilon}_0^{(\lambda_\rho)}, \boldsymbol{\epsilon}^{(\lambda_\rho)}\} \tag{B2}$$

is the ρ meson polarization vector and $\boldsymbol{\sigma}$ is the vector of quark spin Pauli matrices. Expressions in Eq. (B1) are only acceptable in the rest frame of the initial baryon $N(R)$, in which case $\mathbf{p}_4 = -\mathbf{k}$ and $\mathbf{p}_4 = -\mathbf{p}_5$ (see Fig. 8). For the 3rd quark with a nonzero momentum $\mathbf{p}_3 \neq 0$ both expressions do not satisfy the Galilean invariance and the second expression in Eq. (B1) does not correspond to the elementary ρqq vertex $\bar{u}(p_4)\gamma^\mu u(p_3)\rho_\mu(p_3 - p_4)$. Thus, it does not lead to a conserved current in the VMD model.

It is possible to improve the expressions (B1) in an acceptable form without changing them in the rest frame where they were deduced in the $^3P_0$ ansatz. Such corrections are only possible with the substitutions $\mathbf{p}_4 \to \mathbf{p}_4 \pm \mathbf{p}_3$, which become identities for $\mathbf{p}_3 = 0$, i.e., in the rest frame of the third spectator quark.

In our calculations we use the following corrected form of Eq. (B1):

$$\pi qq: \boldsymbol{\sigma} \cdot (\mathbf{p}_4 - \mathbf{p}_3),$$

$$\rho qq: (E_4 + E_3)\boldsymbol{\epsilon}_0^{(\lambda_\rho)} - \{(\mathbf{p}_4 + \mathbf{p}_3) - i[\boldsymbol{\sigma} \times (\mathbf{p}_4 - \mathbf{p}_3)]\} \cdot \boldsymbol{\epsilon}^{(\lambda_\rho)}). \tag{B3}$$

These expressions satisfy Galilean invariance and are well correlated with the Feynman amplitudes $\bar{u}(p_4)\gamma^5 u(p_3)\pi(p_3 - p_4)$ and $\bar{u}(p_4)\gamma^\mu u(p_3)\rho_\mu(p_3 - p_4)$, respectively, (in the nonrelativistic approximation). Here we show that using such a corrected form of Eq. (B1) one can obtain realistic values for the coupling constants ρNN, ωNN, σNN and the nucleon magnetic moments μ_p, μ_n. We further predict the nondiagonal couplings πNR, σNR, ρNR, ωNR starting from a single constant $\gamma = \frac{g_q}{2m_q}$ normalized to the well established value $g_{\pi NN} = 13.5$.

1. Diagonal $N \to N$ transitions

Substituting wave functions (A8)–(A10) into Eq. (11) and taking into account the modification (B3) of Eq. (B1) gives after some algebra the following expressions for the $N \to N + M$ ($N + M \to N$) amplitudes:

$$\begin{aligned} T_{N \to N+\pi}^q &= 3_{nr}\langle\Psi_\pi, \mathbf{k}|\langle\Psi_N, -\mathbf{k}|V_q^{\text{eff}}|\Psi_N, \mathbf{0}\rangle_{nr} \\ &= \frac{5}{3}\left(\frac{g_q}{2m_q}\right)\frac{1}{n^{3/2}(y_\pi)}(8\pi b^2)^{3/4}y_\pi^{3/2}e^{-\zeta(y_\pi)\mathbf{k}^2b^2/6} \\ &\quad \times \left\langle\frac{1}{2}T_z' \Big| \tau_{t_\pi} \Big| \frac{1}{2}T_z\right\rangle\left\langle\frac{1}{2}S_z' \Big| \frac{\boldsymbol{\sigma}\cdot\mathbf{k}}{2m_q} \Big| \frac{1}{2}S_z\right\rangle, \end{aligned} \tag{B4}$$

$$\begin{aligned} T_{N \to N+\sigma}^q &= 3_{nr}\langle\Psi_\sigma, \mathbf{k}|\langle\Psi_N, -\mathbf{k}|V_q^{\text{eff}}|\Psi_N, \mathbf{0}\rangle_{nr} \\ &= -3\left(\frac{g_q}{2m_q}\right)\frac{y_\sigma}{\sqrt{6}(2m_qb)}\frac{1}{n^{5/2}(y_\sigma)}(8\pi b^2)^{3/4}y_\sigma^{3/2} \\ &\quad \times \left(1 + f(y_\sigma)\frac{\mathbf{k}^2b^2}{9}\right)e^{-\zeta(y_\sigma)\mathbf{k}^2b^2/6}\delta_{S_z',S_z}\delta_{T_z',T_z}, \end{aligned} \tag{B5}$$

$$\begin{aligned} T_{\rho+N \to N}^q &= 3_{nr}\langle\Psi_N, \mathbf{0}|V_q^{\text{eff}}|\Psi_N, -\mathbf{k}\rangle|\Psi_\rho, \mathbf{k}, \lambda_\rho, t_\rho\rangle_{nr} \\ &= -\left(\frac{g_q}{2m_q}\right)\frac{1}{n^{3/2}(y_\rho)}(8\pi b^2)^{3/4}y_\rho^{3/2}e^{-\zeta(y_\rho)\mathbf{k}^2b^2/6} \\ &\quad \times \left\langle\frac{1}{2}T_z' \Big| \tau_{t_\rho} \Big| \frac{1}{2}T_z\right\rangle\left[\left(1 + \frac{1}{3}\frac{\mathbf{k}\cdot\boldsymbol{\epsilon}^{(\lambda_\rho)}}{2m_qn(y_\rho)}\right)\delta_{S_z',S_z} \right. \\ &\quad \left. - \frac{5}{3}\left\langle\frac{1}{2}S_z' \Big| \frac{i[\boldsymbol{\sigma}\times\mathbf{k}]\cdot\boldsymbol{\epsilon}^{(\lambda_\rho)}}{2m_q} \Big| \frac{1}{2}S_z\right\rangle\right], \end{aligned} \tag{B6}$$

$$\begin{aligned} T_{\omega+N \to N}^q &= 3_{nr}\langle\Psi_N, \mathbf{0}|V_q^{\text{eff}}|\Psi_N, -\mathbf{k}\rangle|\Psi_\omega, \mathbf{k}, \lambda_\omega\rangle_{nr} \\ &= -\left(\frac{g_q}{2m_q}\right)\frac{1}{n^{3/2}(y_\omega)}(8\pi b^2)^{3/4}y_\omega^{3/2}e^{-\zeta(y_\omega)\mathbf{k}^2b^2/6}\delta_{T_z',T_z} \\ &\quad \times \left[\left(3 + \frac{\mathbf{k}\cdot\boldsymbol{\epsilon}^{(\lambda_\omega)}}{2m_qn(y_\omega)}\right)\delta_{S_z',S_z} - \left\langle\frac{i[\boldsymbol{\sigma}\times\mathbf{k}]\cdot\boldsymbol{\epsilon}^{(\lambda_\omega)}}{2m_q}\right\rangle_S\right]. \end{aligned} \tag{B7}$$

The parameter b is the rms radius of the quark configuration $0s^3$ which is used for the nucleon. The meson radius b_M is related through the relative value

$$y_M = \frac{b_M}{b}, \qquad M = \pi, \sigma, \rho, \ldots, \tag{B8}$$

and we use the notations

$$n(y) = 1 + \frac{2}{3}y^2, \quad \zeta(y) = \frac{1 + 5y^2/6}{n(y)}, \quad f(y) = \frac{1 + y^2/2}{n(y)}. \tag{B9}$$

If $b_R \neq b$ we also use another relative variable $y_R = \frac{b_R}{b}$ and then Eq. (B8) should be generalized as

$$n(y) \to N(y, y_R) = \tfrac{1}{2}(1 + y_R^2) + \tfrac{2}{3}y. \quad \text{(B10)}$$

The strength parameter of the $^3P_0$ model, $\gamma = \frac{g_q}{2m_q}$, is fixed as usual by normalizing the value of the πNN coupling constant to $g_{\pi NN} = 13.5$. From (B4) it follows that

$$g_{\pi NN}^q = \frac{5}{3}\frac{m_N}{m_q}\left(\frac{g_q}{2m_q}\right)\frac{1}{n^{3/2}(y_\pi)}[(8\pi b^2)^{3/4}y_\pi^{3/2}2m_N\sqrt{2M_\pi}] \quad \text{(B11)}$$

and for a typical value of $b = 0.5$ fm one obtains $\gamma \simeq 0.2$.

For the σNN coupling constant

$$g_{\sigma NN}^q = 3\left(\frac{g_q}{2m_q}\right)\frac{y_\sigma}{\sqrt{6}(2m_q b)}\frac{1}{n^{5/2}(y_\sigma)}$$
$$\times [(8\pi b^2)^{3/4}y_\sigma^{3/2}2m_N\sqrt{2M_\sigma}] \quad \text{(B12)}$$

we get

$$g_{\sigma NN}^q = \frac{g_{\pi NN}}{2m_N b}\frac{9\sqrt{3}}{10\sqrt{2}}\sqrt{\frac{M_\sigma}{M_\pi}}\frac{y_\sigma^{5/2}}{y_\pi^{3/2}}\frac{n^{3/2}(y_\pi)}{n^{5/2}(y_\sigma)}, \quad \text{(B13)}$$

taking $g_{\pi NN}^q = g_{\pi NN}$. For typical CQM values of $b = 0.5$ fm and $y_\sigma = y_\pi = 1$ this expression gives a realistic value for the coupling constant with $g_{\sigma NN}^q = 0.262g_{\pi NN} = 3.54$.

For the ρNN coupling constant defined in Eq. (B6) as

$$g_{\rho NN}^q = \frac{1}{3}\left(\frac{g_q}{2m_q}\right)\frac{1}{n^{3/2}(y)}[(8\pi b^2)^{3/4}y^{3/2}2m_N\sqrt{2M_V}], \quad \text{(B14)}$$

substitution of the value $\frac{g_q}{2m_q}$ deduced from Eq. (B11) gives

$$g_{\rho NN}^q = \frac{g_{\pi NN}}{5}\sqrt{\frac{M_\rho}{M_\pi}}\frac{y_\rho^{3/2}}{y_\pi^{3/2}}\frac{n^{3/2}(y_\pi)}{n^{3/2}(y_\rho)} \quad \text{(B15)}$$

and for $y_\rho = y_\pi = 1$ one obtains the realistic value $g_{\rho NN} = g_{\rho NN}^q = 0.469g_{\pi NN} = 6.33$.

Comparing Eqs. (B6) and (B8) one can see that in this approach the ωNN and ρNN couplings are linked by the standard relation

$$g_{\omega NN}^q = 3g_{\rho NN}^q \quad \text{(B16)}$$

which corresponds to "ideal mixing" usually used in the VMD model.

2. Nondiagonal transitions

Here the main objective is the calculation of the non-diagonal baryon matrix elements for the transitions $N + \rho \to R$ and $R \to N + M$. The values of the coupling constants have been fixed by Eqs. (B13), (B15), and (B16), on the basis of $g_{\pi NN}$. We further use them in the expressions for the nondiagonal transitions $N + \gamma^* \to R$, $R \to N + \pi$, $R \to N + \sigma$, etc., substituting symbols $g_{\sigma NN}^q$ and $g_{\rho NN}^q$ (and $g_{\omega NN}^q$ with $g_{\omega NN}^q = 3g_{\rho NN}^q$) instead of the explicit expressions of the right-hand side. of Eqs. (B12) and

(B14). Then the vector-meson absorption amplitude $\mathcal{M}_{V+N\to R}^{q(\lambda_V)} = 2m_N\sqrt{2M_V}T_{V+N\to R}^{q(\lambda_V)}$ is represented by the following two-component column vector:

$$\begin{pmatrix} \mathcal{M}_{\rho+N\to R}^{q(\lambda)} \\ \mathcal{M}_{\omega+N\to R}^{q(\lambda)} \end{pmatrix} = \frac{\sqrt{3}}{2}g_{\rho NN}^q e^{-\zeta(y)k^2b^2/6}\begin{pmatrix} \langle\tfrac{1}{2}T_z'|\tau_{t_\rho}|\tfrac{1}{2}T_z\rangle \\ 3\delta_{T_z',T_z} \end{pmatrix}$$
$$\times \left\{ \left[\left(\epsilon_0^{(\lambda)} + \frac{n_0\tilde{\mathbf{k}}\cdot\boldsymbol{\epsilon}^{(\lambda)}}{2m_N n(y)}\right)p_2(y,\mathbf{k}^2) \right. \right.$$
$$\left. + p_0(y)\frac{n_0\tilde{\mathbf{k}}\cdot\boldsymbol{\epsilon}^{(\lambda)}}{2m_N n(y)} \right] \delta_{S_z',S_z} + \begin{pmatrix} 5 \\ 1 \end{pmatrix}$$
$$\left. \times \left\langle\tfrac{1}{2}S_z'\left|\frac{i[\boldsymbol{\sigma}\times\mathbf{k}]\cdot\boldsymbol{\epsilon}^{(\lambda)}}{2m_N}\right|\tfrac{1}{2}S_z\right\rangle p_2(y,\mathbf{k}^2)\right\}. \quad \text{(B17)}$$

This is the main result of our considerations. Here we use momenta $\mathbf{k} = \mathbf{P} - \mathbf{P}'$, $\tilde{\mathbf{k}} = \mathbf{P} + \mathbf{P}'$, related to momenta $\mathbf{P}$, $\mathbf{P}'$ of initial and final baryon. Only in the rest frame they have the same values, $\tilde{\mathbf{k}} = \mathbf{k}$. In the case $b_R \neq b$ the polynomials $p_{0,2}$ and ζ, n, n_0 also depend on y_R. They are defined by the equations

$$p_0(y) = P_0(y, y_R = 1), \quad p_2(y, \mathbf{q}^2) = P_2(y, y_R = 1, \mathbf{q}^2),$$
$$n_0 = N_0(y_R = 1), \quad N_0(y_R) = \frac{3}{2}y_R^2 - \frac{1}{2},$$
$$\zeta(y) = \tilde{\zeta}(y, y_R = 1), \quad \tilde{\zeta}(y, y_R) = \frac{y_R^2 + \frac{3}{2}(\frac{1+y_R^2}{2} - \frac{4}{9})y^2}{\frac{1+y_R^2}{2} + \frac{2}{3}y^2},$$
$$P_0(y, y_R) = \frac{4}{3}\frac{1+y^2}{N(y, y_R)},$$
$$P_2(y, y_R, \mathbf{k}^2) = \frac{(1-y_R^2)/2 + 2y^2/3}{N(y, y_R)} - y_R^2\left(\frac{1+y^2}{N(y, y_R)}\right)^2\frac{\mathbf{k}^2b^2}{9}, \quad \text{(B18)}$$

with $N(y, y_R)$ defined in Eq. (B10). The $R \to N + \pi$ and $R \to N + \sigma$ decay widths are defined by the matrix elements

$$\mathcal{M}_{R\to N+\pi}^q = 3\langle\Psi_\pi, \mathbf{k}|\langle\Psi_N, -\mathbf{k}|V_q^{\text{eff}}|\Psi_R, \mathbf{0}\rangle$$
$$= \frac{\sqrt{3}}{2}g_{\pi NN}^q p_2(y_\pi, \mathbf{k}^2)e^{-\zeta(y_\pi)k^2b^2/6}$$
$$\times \left\langle\tfrac{1}{2}S_z'|\boldsymbol{\sigma}\cdot\mathbf{k}|\tfrac{1}{2}S_z\right\rangle\left\langle\tfrac{1}{2}T_z'|\tau_{t_\pi}|\tfrac{1}{2}T_z\right\rangle, \quad \text{(B19)}$$

$$\mathcal{M}_{R\to N+\sigma}^q = 3\langle\Psi_\sigma, \mathbf{k}|\langle\Psi_N, -\mathbf{k}|V_q^{\text{eff}}|\Psi_R, \mathbf{0}\rangle$$
$$= \frac{\sqrt{3}}{2}g_{\sigma NN}^q p_4(y_\sigma, \mathbf{k}^2)e^{-\zeta(y_\sigma)k^2b^2/6}\delta_{S_z',S_z}\delta_{T_z',T_z} \quad \text{(B20)}$$

with

$$p_4(y_\sigma, \mathbf{k}^2) = -\frac{2}{3}\frac{1-y_\sigma^2}{n(y_\sigma)} - \frac{\mathbf{k}^2 b^2}{27}\left[\frac{1 + y_\sigma^2/2 + y_\sigma^4/3}{n^2(y_\sigma)}\right.$$
$$\left. + \frac{\mathbf{k}^2 b^2}{3}\frac{(1+y_\sigma^2)(1+y_\sigma^2/2)}{n^3(y_\sigma)}\right]. \tag{B21}$$

As in the case of vector mesons the polynomials $p_2(y_\pi, \mathbf{k}^2)$ and $p_4(y_\sigma, \mathbf{k}^2)$ do not vanish in the limit $|\mathbf{k}| \to 0$ and the nonzero values

$$Z_\pi = \frac{2y_\pi^2/3}{n(y_\pi)}, \qquad Z_\sigma = \frac{2}{3}\frac{1-y_\sigma^2}{n(y_\sigma)}, \tag{B22}$$

determine the amplitudes (B19) and (B20) for small values of $|\mathbf{k}|$.

[1] R. Koniuk and N. Isgur, Phys. Rev. D **21**, 1868 (1980); **23**, 818(E) (1981).
[2] K. Nakamura *et al.* (Particle Data Group), J. Phys. G **37**, 075021 (2010).
[3] A. V. Sarantsev *et al.*, Phys. Lett. B **659**, 94 (2008).
[4] L. Y. Glozman and D. O. Riska, Phys. Rep. **268**, 263 (1996).
[5] I. G. Aznauryan *et al.* (CLAS Collaboration), Phys. Rev. C **80**, 055203 (2009).
[6] V. I. Mokeev, V. D. Burkert, T. S. Lee, L. Elouadrhiri, G. V. Fedotov, and B. S. Ishkhanov (CLAS Collaboration), Phys. Rev. C **80**, 045212 (2009); V. I. Mokeev, JLab Hall B Meeting (2010).
[7] M. B. Gavella, A. Le Yaouanc, L. Oliver *et al.*, Phys. Rev. D **21**, 182 (1980).
[8] Z.-p. Li, V. Burkert, and Z.-j. Li, Phys. Rev. D **46**, 70 (1992).
[9] F. E. Close and Z. P. Li, Phys. Rev. D **42**, 2194 (1990).
[10] S. Capstick and B. D. Keister, Phys. Rev. D **51**, 3598 (1995).
[11] F. Cardarelli, E. Pace, G. Salme, and S. Simula, Phys. Lett. B **397**, 13 (1997); Phys. Lett. B **371**, 7 (1996); Phys. Lett. B **357**, 267 (1995).
[12] I. G. Aznauryan, Phys. Rev. C **76**, 025212 (2007).
[13] D. Robson, Nucl. Phys. **A560**, 389 (1993); U. Meyer, A. J. Buchmann, and A. Faessler, Phys. Lett. B **408**, 19 (1997).
[14] Y. B. Dong, K. Shimizu, A. Faessler, and A. J. Buchmann, Phys. Rev. C **60**, 035203 (1999).
[15] F. Cano and P. Gonzalez, Phys. Lett. B **431**, 270 (1998).
[16] Q. B. Li and D. O. Riska, Phys. Rev. C **74**, 015202 (2006).
[17] V. D. Burkert and T. S. H. Lee, Int. J. Mod. Phys. E **13**, 1035 (2004).
[18] S. Capstick, B. D. Keister, and D. Morel, J. Phys. Conf. Ser. **69**, 012016 (2007).
[19] G. Ramalho and K. Tsushima, Phys. Rev. D **81**, 074020 (2010).
[20] B. Golli, S. Sirca, and M. Fiolhais, Eur. Phys. J. A **42**, 185 (2009).
[21] A. Matsuyama, T. Sato, and T. S. Lee, Phys. Rep. **439**, 193 (2007).
[22] N. Suzuki, T. Sato, and T. S. Lee, Phys. Rev. C **76**, 025205 (2007); arXiv:0910.1742; N. Suzuki, B. Julia-Diaz, H. Kamano *et al.*, Phys. Rev. Lett. **104**, 042302 (2010); B. Julia-Diaz, T. S. Lee, A. Matsuyama, and T. Sato, Phys. Rev. C **76**, 065201 (2007); J. Liu, R. D. McKeown, and M. J. Ramsey-Musolf, Phys. Rev. C **76**, 025202 (2007).
[23] H. Kamano, arXiv:1010.0275.
[24] G. V. Fedotov *et al.* (CLAS Collaboration), Phys. Rev. C **79**, 015204 (2009).
[25] I. G. Aznauryan, V. D. Burkert, G. V. Fedotov, B. S. Ishkhanov, and V. I. Mokeev, Phys. Rev. C **72**, 045201 (2005).
[26] V. I. Mokeev and V. D. Burkert, J. Phys. Conf. Ser. **69**, 012019 (2007).
[27] B. Borasoy, P. C. Bruns, U. G. Meissner, and R. Lewis, Phys. Lett. B **641**, 294 (2006).
[28] D. Djukanovic, J. Gegelia, and S. Scherer, Phys. Lett. B **690**, 123 (2010).
[29] A. W. Thomas, Adv. Nucl. Phys. **13**, 1 (1984).
[30] F. Gross, G. Ramalho, and M. T. Pena, Phys. Rev. C **77**, 015202 (2008); F. Gross, G. Ramalho, and K. Tsushima, Phys. Lett. B **690**, 183 (2010).
[31] O. Krehl, C. Hanhart, S. Krewald, and J. Speth, Phys. Rev. C **62**, 025207 (2000).
[32] E. S. Ackleh, T. Barnes, and E. S. Swanson, Phys. Rev. D **54**, 6811 (1996).
[33] A. Faessler, T. Gutsche, V. E. Lyubovitskij, and Y. L. Ma, Phys. Rev. D **76**, 014005 (2007); A. Faessler, T. Gutsche, S. Kovalenko, and V. E. Lyubovitskij, Phys. Rev. D **76**, 014003 (2007); T. Branz, T. Gutsche, and V. E. Lyubovitskij, Eur. Phys. J. A **37**, 303 (2008); Phys. Rev. D **80**, 054019 (2009); Phys. Rev. D **82**, 054010 (2010); Y. Dong, A. Faessler, T. Gutsche, S. Kovalenko, and V. E. Lyubovitskij, Phys. Rev. D **79**, 094013 (2009); Y. Dong, A. Faessler, T. Gutsche, and V. E. Lyubovitskij, Phys. Rev. D **81**, 014006 (2010); **81**, 074011 (2010); Y. Dong, A. Faessler, T. Gutsche, S. Kumano, and V. E. Lyubovitskij, Phys. Rev. D **82**, 034035 (2010).
[34] Yu. S. Kalashnikova, Phys. Rev. D **72**, 034010 (2005).
[35] L. Micu, Nucl. Phys. **B10**, 521 (1969).
[36] A. Le Yaouanc, L. Oliver, O. Pene, and J.-C. Raynal, Phys. Rev. D **8**, 2223 (1973).
[37] T. Barnes, F. E. Close, P. R. Page, and E. S. Swanson, Phys. Rev. D **55**, 4157 (1997); T. Barnes, N. Black, and P. R. Page, Phys. Rev. D **68**, 054014 (2003); T. Barnes, S. Godfray, and E. S. Swanson, Phys. Rev. D **72**, 054026 (2005).
[38] S. Capstick and W. Roberts, Phys. Rev. D **49**, 4570 (1994).
[39] C. Downum, T. Barnes, J. R Stone, and E. S. Swanson, Phys. Lett. B **638**, 455 (2006).
[40] C. B. Dover, T. Gutsche, M. Maruyama, and A. Faessler, Prog. Part. Nucl. Phys. **29**, 87 (1992).

[41] S. Weinberg, Phys. Rev. **130**, 776 (1963); A. Salam, Nuovo Cimento **25**, 224 (1962).

[42] G. V. Efimov and M. A. Ivanov, *The Quark Confinement Model of Hadrons* (IOP Publishing, Bristol, 1993).

[43] I. V. Anikin, M. A. Ivanov, N. B. Kulimanova, and V. E. Lyubovitskij, Z. Phys. C **65**, 681 (1995); M. A. Ivanov, M. P. Locher, and V. E. Lyubovitskij, Few-Body Syst. **21**, 131 (1996); M. A. Ivanov, V. E. Lyubovitskij, J. G. Körner, and P. Kroll, Phys. Rev. D **56**, 348 (1997); A. Faessler, T. Gutsche, M. A. Ivanov, J. G. Korner, A. Faessler, T. Gutsche, B. R. Holstein, M. A. Ivanov, J. G. Korner, and V. E. Lyubovitskij, Phys. Rev. D **78**, 094005 (2008); A. Faessler, T. Gutsche, M. A. Ivanov, J. G. Korner, and V. E.

Lyubovitskij, Phys. Rev. D **80**, 034025 (2009); T. Branz, A. Faessler, T. Gutsche, M. A. Ivanov, J. G. Korner, V. E. Lyubovitskij, and B. Oexl, Phys. Rev. D **81**, 114036 (2010).

[44] N. M. Kroll, T. D. Lee, and B. Zumino, Phys. Rev. **157**, 1376 (1967).

[45] H. J. Weber, Phys. Rev. C **41**, 2783 (1990).

[46] S. Capstick *et al.*, Eur. Phys. J. A **35**, 253 (2008).

[47] T. Barnes and S. Swanson, Phys. Rev. C **77**, 055206 (2008).

[48] S. Mandelstam, Ann. Phys. (N.Y.) **19**, 1 (1962).

[49] J. Terning, Phys. Rev. D **44**, 887 (1991).

[50] J. J. Kelly, Phys. Rev. C **70**, 068202 (2004).

[51] M. N. Achasov *et al.*, Phys. Lett. B **537**, 201 (2002).